THE BALTIC JOURNAL
OF ROAD AND BRIDGE ENGINEERING
2026/21(3)

ISSN 1822-427X/eISSN 1822-4288
2026 Volume 21 Issue 3: 19–40
https://doi.org/10.7250/bjrbe.2026-21.681

STUDY ON VALIDITY OF MAXIMUM STATIC FRICTION COEFFICIENT AS AN EVALUATION VALUE FOR SKID-RESISTANCE OF PAVEMENT SURFACE

KEI YAMAMOTO[1,*], OSAMU TAKAHASHI[2]

[1] *Gaeart Co., Ltd., Japan*

[2] *Nagaoka University of Technology, Niigata, Japan*

Received 7 January 2026; accepted 28 August 2026

Abstract. The skid resistance of a pavement surface is a critical indicator of driving safety, typically quantified by the dynamic friction coefficient measured using a Friction Measurement Vehicle or a Dynamic Friction Tester. The dynamic friction coefficient is calculated from the dynamic friction force acting on a rubber slider in a sliding state, directly influencing the braking distance before a tire stops sliding. In this study, we hypothesize that the resistance force before a tire begins to slip – rather than the braking distance – is more closely related to traffic accident risk. Therefore, this study focuses on the maximum static friction coefficient, representing the resistance force at the onset of tire sliding. Maximum static friction coefficients were measured across various road surfaces and compared with dynamic friction coefficients to evaluate their relationship with accident risk. The results demonstrate that the maximum static friction coefficient provides a more realistic evaluation of road surface skid resistance.

Keywords: dynamic friction, friction, friction characteristic, pavement, skid-resistance, static friction.

* Corresponding author. E-mail: keiyamamoto@gaeart.com

Introduction

Traffic safety is a fundamental requirement of pavement design. Skid resistance plays a vital role in ensuring safe, smooth, and comfortable vehicle travel. It is generally evaluated using either the skid friction coefficient, measured by a friction measurement vehicle, or the dynamic friction coefficient, measured by a device such as a Dynamic Friction Tester (DFT).

Both the skid friction coefficient and the dynamic friction coefficient are calculated from the friction force generated when a test tire or rubber slider moves across the road surface. These parameters are directly related to the sliding distance of a fully locked tire.

Vehicle skidding typically occurs when tires lock up during hard braking on straight road sections, or when centrifugal force acts on the vehicle while negotiating a curve. In these scenarios, the skid and dynamic friction coefficients are used to evaluate the sliding distance after tire lockup, as well as the lateral drift toward the outside of a curve. However, because modern vehicles are equipped with anti-lock braking systems (ABS) to prevent tire lockup, straight-line skidding under full lockup has become increasingly rare (Figure 1).

On curved road sections, however, vehicles remain at risk of slipping and drifting out of their lane, potentially leading to severe collisions with oncoming traffic or roadside structures (Figure 2). Therefore, evaluating pavement safety – particularly on curves – requires assessing not only the total slip distance, but also the frictional behavior immediately preceding the onset of slipping.

While numerous studies have investigated tire friction during active sliding, research focusing on road surface friction at the exact threshold where slipping initiates remains limited (Hirasawa, 2003; Saito, 2003).

This study focuses on the maximum static friction coefficient observed during the transition of a tire from rolling to sliding. Both the dynamic friction coefficient and the maximum static friction coefficient were measured across various pavement surface textures. The differences between these two parameters were subsequently analyzed to evaluate their respective validity for pavement skid resistance assessment.

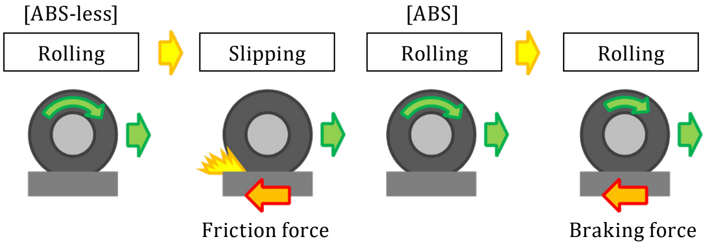

Figure 1. Comparison between tires without and with ABS

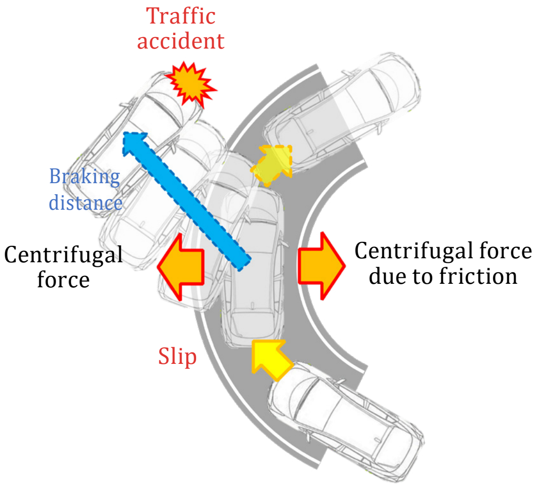

Figure 2. Situations leading to skidding on curved roads

1. Literature review

1.1. Pavement skid resistance

Numerous studies have reported a strong correlation between pavement skid resistance and the frequency of traffic accidents (Wallman & Åström, 2001). When road surface friction falls below a certain threshold, the number of collision accidents on wet roads increases significantly. Specifically, if road surface friction is reduced by half, the risk of collision accidents doubles (Viner et al., 2004).

Pavement surface friction is significantly influenced by its surface texture. Pavement surface textures are classified into three categories – microtexture, macrotexture, and megatexture – based on wavelength and amplitude; surface irregularities with wavelengths exceeding that of megatexture are referred to as roughness (Wambold et al., 1995). Microtexture refers to texture with a wavelength of 0.5 mm or less, macrotexture to texture with a wavelength of 0.5 to 50 mm, and megatexture to texture with a wavelength of 50 to 500 mm. Road surface friction is influenced by microtexture and macrotexture. These textures vary depending on the type, dimensions, and particle size distribution of the aggregates. Microtexture depends on the mineralogy and surface roughness of the aggregate particles, whereas macrotexture is governed by the aggregate gradation and mix design (Hall et al., 2009).

1.2. Friction mechanisms between tire and pavement surfaces

The friction between the tire and the road surface primarily consists of two components: adhesion and hysteresis. Adhesion arises from intermolecular bonding and shear stress at the tire-pavement interface, whereas hysteresis is the energy dissipation caused by the repeated deformation and recovery of the tire rubber as it conforms to surface irregularities (Hall et al., 2009).

As shown in Figure 3, a tire on the road surface is modelled as a rotating wheel (a rigid body), a carcass supported by inflation pressure (acting as a spring), and tread rubber (an elastic body). The carcass and tread rubber deform under vehicle loads and wheel rotation. This deformation results in a speed difference between the vehicle's forward motion and the circumferential rotation of the tread rubber. Consequently, relative displacement occurs between the carcass and the tread rubber (Sakai, 1979). Based on the relative displacement resulting from the deformation of the carcass and tread rubber, the circumferential force generated by the tire in the absence of slip is expressed by the following equation:

$$f_x = C_x \frac{\Delta d}{d} x, \tag{1}$$

where
f_x is the circumferential force exerted by the tire on the road surface;
C_x is the circumferential stiffness of the tread rubber;
d is the distance from the leading edge of the contact patch;
Δd is the relative displacement caused by the velocity difference between the tread rubber and the road surface, and
x is the distance traveled along the contact patch.

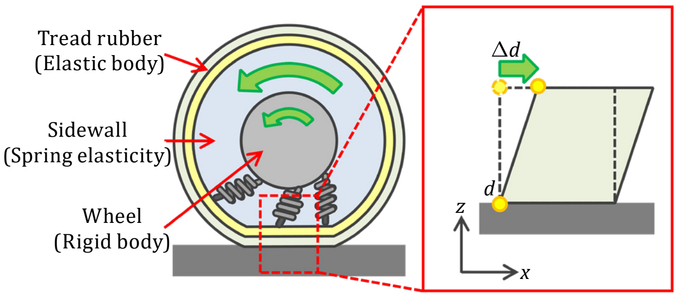

Figure 3. Tire structure and deformation during rolling on a road surface

Generally, friction force is modelled as proportional to the applied normal load. In addition to the vehicle load, the vertical force – influenced by the inflation pressure of the carcass – exhibits a parabolic distribution, as shown in Figure 4. The frictional force in this case is expressed by the following equations, depending on the presence or absence of tire slip.

$$F_x' = f_z \times \mu_S, \quad (2)$$

$$F_x'' = f_z \times \mu_D, \quad (3)$$

where
F_x' is the maximum friction force when the tire is not slipping;
F_x'' is the kinetic friction force when the tire is slipping;
f_z is the vertical load acting on the road surface;
μ_S is the maximum static friction coefficient under non-slipping conditions, and
μ_D is the coefficient of kinetic friction under slipping conditions.

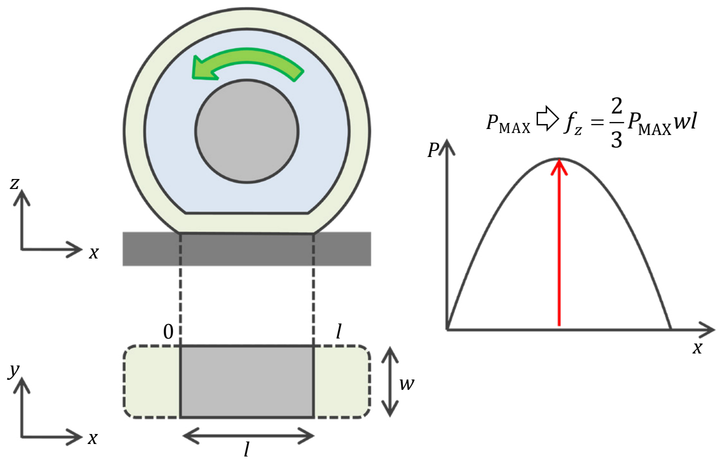

Figure 4. Contact pressure distribution of a rolling tire on a road surface

The frictional force generated across the tire-pavement contact area can be calculated using Equations (1)–(3). Figure 5 illustrates the calculated frictional force derived from the circumferential and vertical forces acting on the tread rubber.

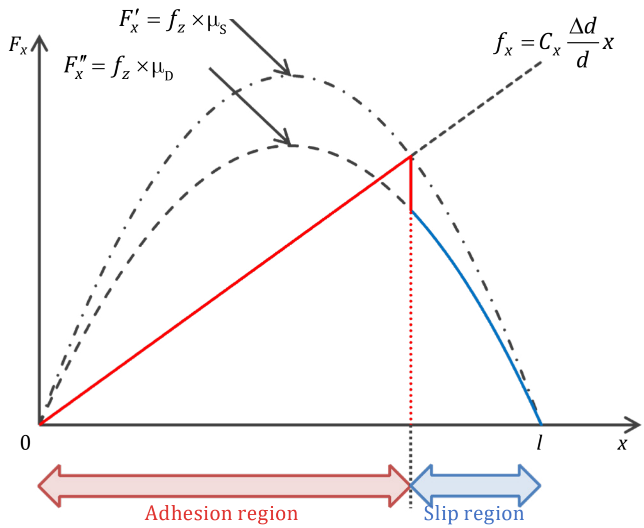

Figure 5. Circumferential friction force acting on a rolling tire contact area

Furthermore, when the tire operates at a slip angle relative to the direction of travel, the contact patch deforms as shown in Figure 6. Consequently, a lateral force is generated due to tire deformation and the frictional force within the adhesion region. This lateral force enables the vehicle to turn.

The driving or braking force of a tire is transmitted through the adhesion region. As the adhesion region shrinks and the sliding region expands, the lateral force decreases. When the lateral force falls below the centrifugal force, the tire begins to slide.

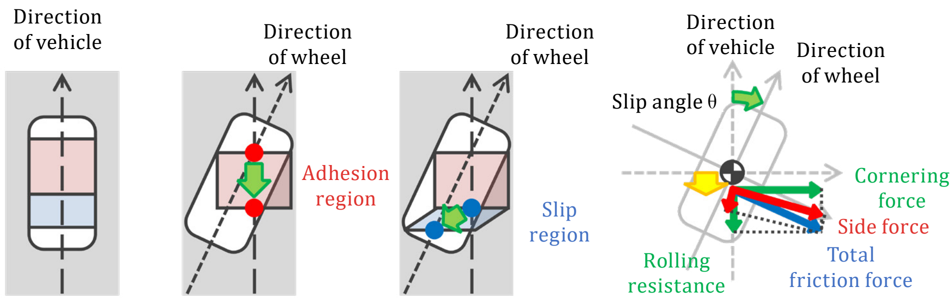

Figure 6. Friction forces acting on the tire contact patch during cornering

1.3. Friction evaluation method

Pavement surface friction measurement methods are broadly categorised into longitudinal and lateral friction evaluations. Longitudinal skid friction is typically measured using the locked-wheel or slip method, whereas lateral friction is evaluated using the side-force method.

In the locked-wheel method, the tire travels in the direction of vehicle motion, and the frictional force is measured when the tire is fully locked (Henry, 2000; ASTM E274, 2020). When a difference exists between the vehicle speed and the tire rotational speed, the condition corresponds to sliding friction defined by a specific slip ratio; the slip method measures friction at a controlled slip ratio (Henry, 2000). Thus, a fully locked tire corresponds to a slip ratio of 100%. Slip methods include fixed-slip ratio methods – such as the Scottish GripTester and the Swedish Saab Friction Tester (SFT) – and variable-slip ratio methods, such as the Norwegian Norsemeter and the French IMAG. Meanwhile, the side-force method measures the lateral force generated when a test wheel is set at a slip angle relative to the vehicle's direction of travel (Henry, 2000).

Some of these measuring devices can also perform measurements using actual vehicle-fitted tires. Generally, measurements taken with ribbed tires are heavily influenced by the microtexture of the road surface, whereas those taken with slick tires primarily reflect the macrotexture and water drainage performance (Li et al., 2005).

Small-scale devices also offer a simple way to measure pavement friction using a rubber slider. Common examples include the British Pendulum Tester (BPT) developed in the UK and the Dynamic Friction Tester (DFT) from Japan. In the BPT, a pendulum fitted with a rubber slider is released from a fixed height to slide over the surface over a designated distance, losing kinetic energy due to friction. The loss of energy prevents the pendulum from returning to its original height, and friction is evaluated based on this height difference (Giles, 1964). Pavement friction is strongly dependent on sliding speed. As the BPT operates at a low sliding speed of approximately 10 km/h – making it highly sensitive to microtexture – it serves as an indicator of surface microtexture characteristics. In contrast, the DFT measures friction by spinning a rubber-slider-equipped disc and bringing it into contact with the road surface. As friction decelerates the rotating disc, the device can measure friction across a range of sliding speeds (Abe, 2000; ASTM E1911, 2019).

In recent years, integrated evaluations combining road surface texture and friction – measured via laser scanners – have gained traction (Smadi & Alhasan, 2025). Regarding human walking, it has been reported that evaluating the coefficient of kinetic friction when the foot slips, along with the coefficient of static friction when the foot pushes off without slipping, can be effective. Consequently, static friction measurement is often employed to assess pedestrian walkway safety (Brungraber, 1976).

2. Test overview

2.1. Type of pavement surface

The tests in this study were conducted using specimens (400 × 400 mm, 50 mm thick) prepared with a roller compactor. The specimens comprised asphalt pavements – including three dense-graded, three porous, and two gap-graded mixtures – and concrete pavements with four different surface finishes. A complete list of specimens is provided in Table 1.

Table 1. Types of specimens used in the tests

Symbol	Type of Mixture	Note
D-1	Dense-Graded Asphalt Mixture (MAS: 13 mm)	Straight-asphalt (Penetration 60-80)
D-2	Dense-Graded Asphalt Mixture (MAS: 13 mm)	Polymer Modified Asphalt (Type II)
D-3	Fine-Graded Asphalt Mixture (MAS: 13 mm)	Polymer Modified Asphalt (Type II)
P-1	Porous Asphalt Mixture (NMAS: 13 mm)	Air Void ratio is 20 percent
P-2	Porous Asphalt Mixture (NMAS: 13 mm)	Air Void ratio is 17 percent
P-3	Porous Asphalt Mixture (NMAS: 5 mm)	Air Void ratio is 17 percent
G-1	Stone Mastic Asphalt Mixture (NMAS: 13 mm)	Air Void ratio is 2.5 percent
G-2	Stone Mastic Asphalt Mixture (NMAS: 13 mm)	Air Void ratio is 7 percent
C-1	Concrete Pave (Trowel-finish)	Nominal Maximum Aggregate Size: 20 mm
C-2	Concrete Pave (Broom-finish)	Flexural Strength: 4.5 MPa
C-3	Concrete Pave (Exposed-aggregate)	Water-Cement Ratio: 47.2 percent
C-4	Concrete Pave (Groove Method)	Age: 28-days (Moist-cured specimens)

For the dense-graded type, the effects of binder type were evaluated by comparing straight asphalt (StAs) and polymer-modified asphalt (PMA), while grading differences were compared between standard dense-graded and fine-graded mixtures (Figure 7). For porous asphalt mixtures, air void ratios of 20% and 17% were compared, alongside maximum aggregate sizes of 13 mm and 5 mm (Figure 8). For gap-graded mixtures, smooth and rough surfaces were prepared by varying the mortar volume within the voids in mineral aggregate (VMA) (Figure 9).

Figure 7. Surfaces of dense-graded and fine-graded asphalt mixtures

Figure 8. Surfaces of porous asphalt mixtures with air void ratios of 20% and 17%, and maximum aggregate sizes of 13 mm and 5 mm

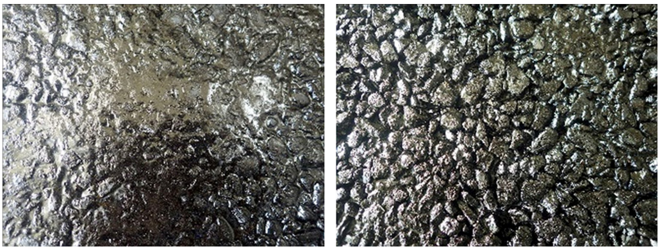

Figure 9. Surfaces of gap-graded asphalt mixtures with smooth and rough surface textures

For the concrete pavements, a smooth surface with a trowel finish and a rough surface with a broom finish were prepared. Additionally, an exposed-aggregate surface – created by removing the surface mortar – and a surface with longitudinal grooves were prepared (Figure 10).

Figure 10. Surfaces of concrete pavement, trowel-finished, broom-finished, exposed-aggregate, and longitudinal groove

2.2. Measurement methods for dynamic and maximum static friction coefficients

The dynamic friction coefficient was measured using a DFT in accordance with the Manual of Pavement Test Methods (Japan Road Association S021-1, 2019). The sliding speeds of the DFT were set to 20, 40, 60, and 80 km/h (equivalent to vehicle driving speeds). Measurements were repeated four times under dry conditions, and the average of the second to fourth measurements was adopted as the representative dynamic friction coefficient for each surface.

The maximum static friction coefficient was calculated based on the Coulomb friction model, as illustrated in Figure 11. A vertical weight was applied to a rubber specimen, which was then pulled horizontally to measure the maximum tensile force at the onset of sliding. The maximum static friction coefficient was determined using Equation (4):

$$\mu_S = \frac{T_{MAX}}{W}, \tag{4}$$

where

μ_S is the maximum static friction coefficient between the test rubber specimen and the pavement surface;

T_{MAX} is the maximum tensile force at the onset of sliding (N), and

W is the applied vertical load (N).

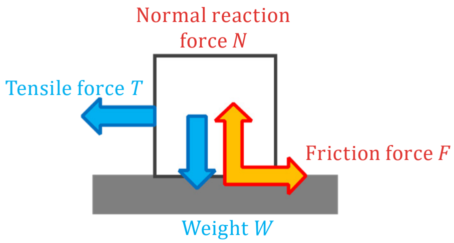

Figure 11. Schematic diagram of the Coulomb friction model

A device based on this principle is the Portable Push-Pull Skid Resistance Tester (ONO-PPSM) (Ono, 2004). Although this device is typically used to evaluate the skid resistance of sidewalks and flooring materials for walking conditions, this study utilised it to assess pavement surfaces, specifically focusing on its static friction measurement capability. A test rubber specimen with dimensions of 60 mm (length) ×50 mm (width) ×3 mm (thickness) and a Shore hardness of 80 was used. Measurements were conducted on a dry surface under a vertical load of 98 N (10 kg) and a tensile loading rate of 254 N/s. Measurements were repeated five times in both the longitudinal and transverse directions, and the average value was calculated for each direction. The mean of these two averages was adopted as the representative maximum static friction coefficient for each surface. Figure 12 shows the DFT and ONO-PPSM devices used in this study.

Figure 12. Photographs of the DFT and ONO-PPSM device

The dynamic friction coefficient and the maximum static friction coefficient were measured at a pavement surface temperature of 20 °C. Table 2 summarises the measurement repeatability on pavement surfaces evaluated using the DFT and ONO-PPSM. High repeatability was confirmed for both measurement methods.

Table 2. Coefficients of variation of measurement results

	Dynamic friction coefficient (DFT)				Maximum static friction coefficient
	20 km/h	40 km/h	60 km/h	80 km/h	
CV	2.7%	1.8%	1.7%	1.8%	3.6%

3. Test result

3.1. Dynamic friction coefficient

Figure 13 presents the dynamic friction coefficients obtained using the DFT. Furthermore, statistical significance tests were performed to compare the results, adopting a two-tailed significance level of α = 0.05. The findings are summarised in Table 3.

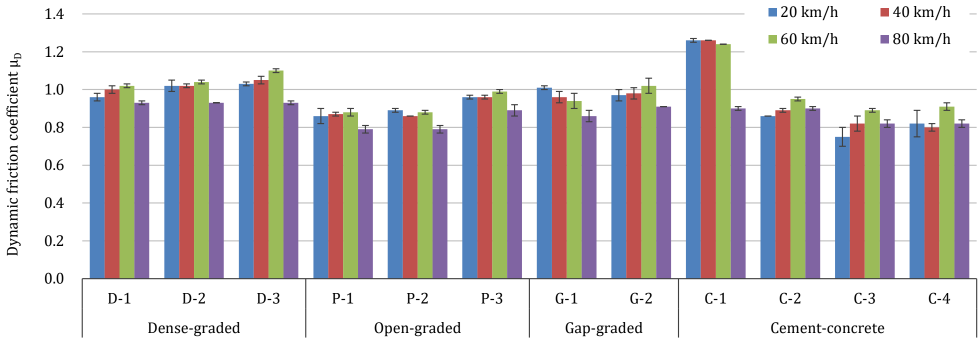

Figure 13. Dynamic friction coefficients at various sliding speeds

Table 3. List of p-values from Significance Tests (Dynamic friction coefficient)

(Sliding speed = 20 km/h)

20 km/h	D-2	D-3	P-1	P-2	P-3	G-1	G-2	C-1	C-2	C-3	C-4
D-1	≥ 0.05	< 0.05	< 0.05	< 0.05	≥ 0.05	< 0.05	≥ 0.05	< 0.05	< 0.05	< 0.05	≥ 0.05
D-2	-	≥ 0.05	< 0.05	< 0.05	≥ 0.05	≥ 0.05	≥ 0.05	< 0.05	< 0.05	< 0.05	< 0.05
D-3	-	-	< 0.05	< 0.05	< 0.05	≥ 0.05	≥ 0.05	< 0.05	< 0.05	< 0.05	< 0.05
P-1	-	-	-	≥ 0.05	≥ 0.05	< 0.05	< 0.05	< 0.05	≥ 0.05	< 0.05	≥ 0.05
P-2	-	-	-	-	< 0.05	< 0.05	< 0.05	< 0.05	< 0.05	< 0.05	≥ 0.05
P-3	-	-	-	-	-	< 0.05	≥ 0.05	< 0.05	< 0.05	< 0.05	≥ 0.05
G-1	-	-	-	-	-	-	≥ 0.05	< 0.05	< 0.05	< 0.05	< 0.05
G-2	-	-	-	-	-	-	-	< 0.05	< 0.05	< 0.05	< 0.05
C-1	-	-	-	-	-	-	-	-	< 0.05	< 0.05	< 0.05
C-2	-	-	-	-	-	-	-	-	-	≥ 0.05	≥ 0.05
C-3	-	-	-	-	-	-	-	-	-	-	≥ 0.05

(Sliding speed = 40 km/h)

40 km/h	D-2	D-3	P-1	P-2	P-3	G-1	G-2	C-1	C-2	C-3	C-4
D-1	≥ 0.05	< 0.05	< 0.05	< 0.05	≥ 0.05	≥ 0.05	≥ 0.05	< 0.05	< 0.05	< 0.05	< 0.05
D-2	-	< 0.05	< 0.05	< 0.05	< 0.05	≥ 0.05	≥ 0.05	< 0.05	< 0.05	< 0.05	< 0.05
D-3	-	-	< 0.05	< 0.05	< 0.05	< 0.05	< 0.05	< 0.05	< 0.05	< 0.05	< 0.05
P-1	-	-	-	< 0.05	< 0.05	< 0.05	< 0.05	< 0.05	< 0.05	≥ 0.05	< 0.05
P-2	-	-	-	-	< 0.05	< 0.05	< 0.05	< 0.05	< 0.05	≥ 0.05	< 0.05
P-3	-	-	-	-	-	≥ 0.05	≥ 0.05	< 0.05	< 0.05	< 0.05	< 0.05
G-1	-	-	-	-	-	-	≥ 0.05	< 0.05	≥ 0.05	< 0.05	< 0.05
G-2	-	-	-	-	-	-	-	< 0.05	< 0.05	< 0.05	< 0.05
C-1	-	-	-	-	-	-	-	-	< 0.05	< 0.05	< 0.05
C-2	-	-	-	-	-	-	-	-	-	≥ 0.05	< 0.05
C-3	-	-	-	-	-	-	-	-	-	-	≥ 0.05

(Sliding speed = 60 km/h)

60 km/h	D-2	D-3	P-1	P-2	P-3	G-1	G-2	C-1	C-2	C-3	C-4
D-1	≥ 0.05	< 0.05	< 0.05	< 0.05	< 0.05	≥ 0.05	≥ 0.05	< 0.05	< 0.05	< 0.05	< 0.05
D-2	-	< 0.05	< 0.05	< 0.05	< 0.05	≥ 0.05	≥ 0.05	< 0.05	< 0.05	< 0.05	< 0.05
D-3	-	-	< 0.05	< 0.05	< 0.05	< 0.05	≥ 0.05	< 0.05	< 0.05	< 0.05	< 0.05
P-1	-	-	-	≥ 0.05	< 0.05	≥ 0.05	< 0.05	< 0.05	< 0.05	≥ 0.05	≥ 0.05
P-2	-	-	-	-	< 0.05	≥ 0.05	< 0.05	< 0.05	< 0.05	≥ 0.05	< 0.05
P-3	-	-	-	-	-	≥ 0.05	≥ 0.05	< 0.05	< 0.05	< 0.05	< 0.05
G-1	-	-	-	-	-	-	≥ 0.05	< 0.05	≥ 0.05	≥ 0.05	≥ 0.05
G-2	-	-	-	-	-	-	-	< 0.05	≥ 0.05	< 0.05	< 0.05
C-1	-	-	-	-	-	-	-	-	< 0.05	< 0.05	< 0.05
C-2	-	-	-	-	-	-	-	-	-	< 0.05	< 0.05
C-3	-	-	-	-	-	-	-	-	-	-	≥ 0.05

(Sliding speed = 80 km/h)

80 km/h	D-2	D-3	P-1	P-2	P-3	G-1	G-2	C-1	C-2	C-3	C-4
D-1	≥ 0.05	≥ 0.05	< 0.05	< 0.05	≥ 0.05	≥ 0.05	< 0.05	< 0.05	< 0.05	< 0.05	< 0.05
D-2	-	≥ 0.05	< 0.05	< 0.05	≥ 0.05	≥ 0.05	< 0.05	< 0.05	< 0.05	< 0.05	< 0.05
D-3	-	-	< 0.05	< 0.05	≥ 0.05	≥ 0.05	≥ 0.05	< 0.05	< 0.05	< 0.05	< 0.05
P-1	-	-	-	≥ 0.05	< 0.05	< 0.05	< 0.05	< 0.05	< 0.05	≥ 0.05	≥ 0.05
P-2	-	-	-	-	< 0.05	< 0.05	< 0.05	< 0.05	< 0.05	≥ 0.05	< 0.05
P-3	-	-	-	-	-	≥ 0.05	≥ 0.05	≥ 0.05	≥ 0.05	< 0.05	≥ 0.05
G-1	-	-	-	-	-	-	≥ 0.05	≥ 0.05	≥ 0.05	≥ 0.05	≥ 0.05
G-2	-	-	-	-	-	-	-	≥ 0.05	≥ 0.05	< 0.05	< 0.05
C-1	-	-	-	-	-	-	-	-	≥ 0.05	< 0.05	< 0.05
C-2	-	-	-	-	-	-	-	-	-	< 0.05	< 0.05
C-3	-	-	-	-	-	-	-	-	-	-	≥ 0.05

Based on these results, although the trends varied by pavement type at sliding speeds of 20 to 60 km/h, the dynamic friction coefficient consistently decreased at 80 km/h across all surfaces.

For the dense-graded types (D-1, D-2, and D-3), no significant difference in the dynamic friction coefficient was observed between StAs (D-1) and PMA (D-2), suggesting that the binder type had minimal effect. Furthermore, no substantial difference was identified between the dense-graded mixture (D-2) and the fine-graded mixture (D-3). For these mixtures, the dynamic friction coefficient increased slightly as the sliding speed increased from 20 km/h to 60 km/h, but decreased at 80 km/h.

For the porous mixtures (P-1, P-2, and P-3), no significant difference in the dynamic friction coefficient was observed between the 20% porosity (P-1) and 17% porosity (P-2) specimens, indicating that porosity had a minimal effect. On the other hand, the specimen with a maximum aggregate size of 5 mm (P-3) exhibited a higher dynamic friction coefficient than that with a 13 mm maximum aggregate size (P-2), suggesting that maximum aggregate size has a more dominant influence than porosity. With respect to sliding speed, the dynamic friction coefficient showed little variation between 20 and 60 km/h, but decreased at 80 km/h.

For the gap-graded mixtures (G-1 and G-2), no significant differences were observed, with their dynamic friction coefficients ranging between those of the porous and dense-graded mixtures. They exhibited a trend similar to the other pavement surfaces, showing a decrease in the coefficient at a sliding speed of 80 km/h.

Among the concrete pavements (C-1, C-2, C-3, and C-4), the trowel-finished surface (C-1) exhibited the highest dynamic friction coefficient. This coefficient tended to increase slightly as the sliding speed increased from 20 to 60 km/h, before decreasing at 80 km/h.

Among the concrete pavements (C-1, C-2, C-3, and C-4), the trowel-finished surface (C-1) exhibited the highest dynamic friction coefficient. This coefficient tended to increase slightly as the sliding speed increased from 20 to 60 km/h, before decreasing at 80 km/h.

3.2. Maximum static friction coefficient

Figure 14 presents the maximum static friction coefficients measured using the ONO-PPSM. Furthermore, statistical significance tests were performed to compare the results, as summarised in Table 4.

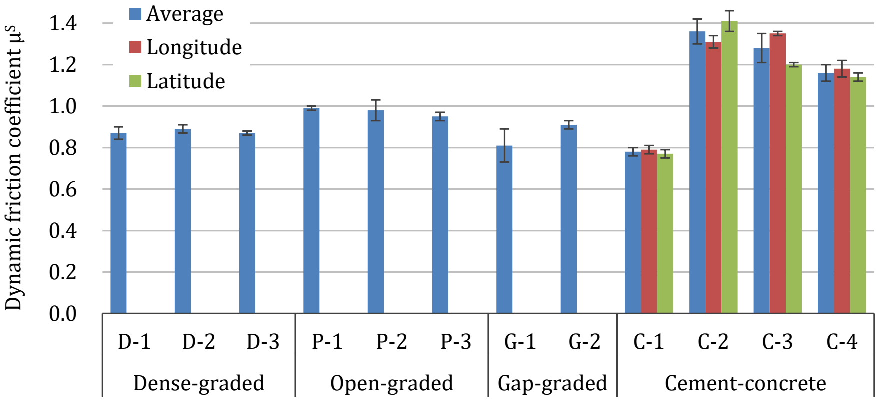

Figure 14. Maximum static friction coefficients

Table 4. List of p-values from significance tests (Maximum static friction coefficient)

	D-2	**D-3**	**P-1**	**P-2**	**P-3**	**G-1**	**G-2**	**C-1**	**C-2**	**C-3**	**C-4**
D-1	≥ 0.05	≥ 0.05	< 0.05	< 0.05	< 0.05	≥ 0.05	< 0.05	< 0.05	< 0.05	< 0.05	< 0.05
D-2	-	< 0.05	< 0.05	< 0.05	< 0.05	< 0.05	< 0.05	< 0.05	< 0.05	< 0.05	< 0.05
D-3	-	-	< 0.05	< 0.05	< 0.05	≥ 0.05	< 0.05	< 0.05	< 0.05	< 0.05	< 0.05
P-1	-	-	-	≥ 0.05	< 0.05	< 0.05	< 0.05	< 0.05	< 0.05	< 0.05	< 0.05
P-2	-	-	-	-	≥ 0.05	< 0.05	< 0.05	< 0.05	< 0.05	< 0.05	< 0.05
P-3	-	-	-	-	-	< 0.05	< 0.05	< 0.05	< 0.05	< 0.05	< 0.05
G-1	-	-	-	-	-	-	< 0.05	≥ 0.05	< 0.05	< 0.05	< 0.05
G-2	-	-	-	-	-	-	-	< 0.05	< 0.05	< 0.05	< 0.05
C-1	-	-	-	-	-	-	-	-	< 0.05	< 0.05	< 0.05
C-2	-	-	-	-	-	-	-	-	-	< 0.05	< 0.05
C-3	-	-	-	-	-	-	-	-	-	-	< 0.05

For the dense-graded types (D-1, D-2, and D-3), no significant difference in the maximum static friction coefficient was observed between StAs (D-1) and PMA (D-2), indicating that the binder type had a minimal effect. Furthermore, the difference between the dense-graded mixture (D-2) and the fine-graded mixture (D-3) was negligible, suggesting that aggregate gradation has no substantial impact.

For the porous mixtures (P-1, P-2, and P-3), the difference in the maximum static friction coefficient between the 20% porosity (P-1) and 17% porosity (P-2) specimens was minimal and not statistically significant, indicating that porosity had little effect. Furthermore, the specimen with a maximum aggregate size of 5 mm (P-3) exhibited a slightly lower maximum static friction coefficient than that with a 13 mm size (P-2).

For the gap-graded mixtures (G-1 and G-2), SMA (G-1) – where aggregate voids are filled with mortar – exhibited a lower maximum static friction coefficient than functional SMA (G-2), which possesses a coarser surface texture. Furthermore, although their surface profiles were comparable, functional SMA (G-2) – characterised by a slightly higher mortar content and finer texture – showed a statistically significant difference in maximum static friction coefficient compared to the porous mixtures (P-1 and P-2), though the magnitude of this difference was small.

For the concrete pavements (C-1, C-2, C-3, and C-4), statistically significant differences were observed across all cases. The trowel-finished surface (C-1) exhibited the lowest maximum static friction coefficient, whereas surfaces with rougher textures yielded higher values. Furthermore, the broom finish (C-2) and the grooved surface (C-4) possessed directional surface irregularities: the broom finish featured transverse markings, while the grooving method combined a transverse broom finish with longitudinal grooves. Comparing the maximum static friction coefficients relative to these directions revealed higher values in the transverse direction for the broom finish (C-2) and in the longitudinal direction for the grooving method (C-4).

Measurements of the maximum static friction coefficient across various pavement surfaces revealed clear distinctions based on surface type. Although variations in the coefficient were observed between the dense-graded and porous pavement categories, no statistically significant differences were attributable to variations in aggregate gradation, binder type, or maximum aggregate size within these categories. In contrast, significant differences in the maximum static friction coefficient were observed for gap-graded and concrete pavements, depending on their surface texture and finishing method.

3.3. Relationship between dynamic friction coefficient and maximum static friction coefficient

The measured dynamic friction coefficients were compared with the maximum static friction coefficients to evaluate the characteristics and differences of each parameter. Figure 15 compares the maximum static friction coefficients with the dynamic friction coefficients measured at sliding speeds of 20 km/h (low-speed regime) and 80 km/h (high-speed regime).

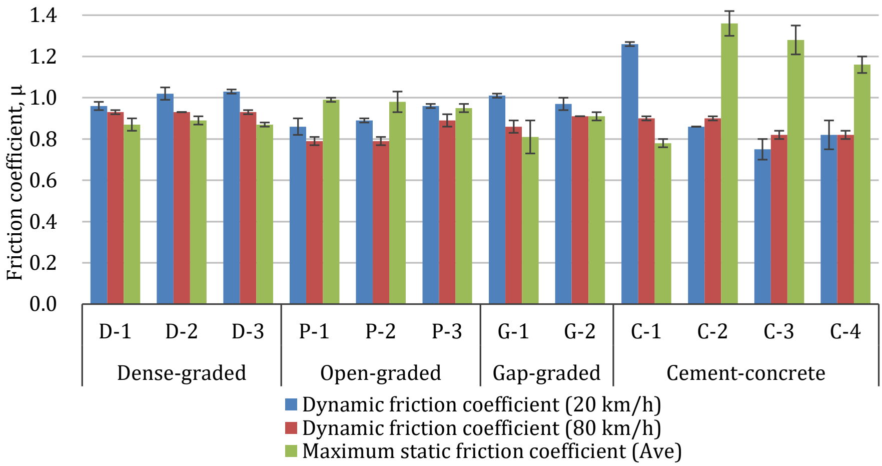

Figure 15. Comparison between dynamic friction coefficients and maximum static friction coefficient

The dynamic friction coefficient was high for pavement surfaces with smooth textures and minimal macro-texture irregularities (e.g., D-1, D-2, D-3, P-3, and C-1), but low for surfaces with rough textures and pronounced irregularities (e.g., P-1, P-2, C-2, C-3, and C-4). Conversely, the maximum static friction coefficient was low for smooth surfaces with minimal irregularities (e.g., D-1, D-2, D-3, P-3, G-1, and C-1) and high for rough surfaces with pronounced irregularities (e.g., P-1, P-2, G-2, C-2, C-3, and C-4). These results demonstrate that the dynamic and maximum static friction coefficients exhibit contrasting trends with respect to surface texture irregularities.

In the DFT, the frictional force is measured as a rubber test specimen slides across the pavement surface. Previous studies noted that the dynamic friction coefficient is lower for porous surfaces – where the contact frequency (or contact area) with surface asperities is reduced – and higher for dense-graded surfaces, where the contact with asperities is more extensive. The results of the present study are consistent with these findings (Ichihara, 1969; Onoda, 2003). In contrast, when using portable skid resistance testers, the rubber specimen deforms under the applied load, causing it to penetrate into surface irregularities. This deformation-induced penetration increases the frictional force, likely leading to a higher maximum static friction coefficient on rough surfaces with pronounced irregularities. This phenomenon is known as “plowing friction,” which is generally considered to have a minimal effect on dynamic friction evaluation (Hall et al., 2009). However, our measurement results suggest that the maximum static friction coefficient is indeed influenced by plowing friction.

Figure 16 illustrates the relationship between the dynamic friction coefficient and the maximum static friction coefficient at different sliding speeds.

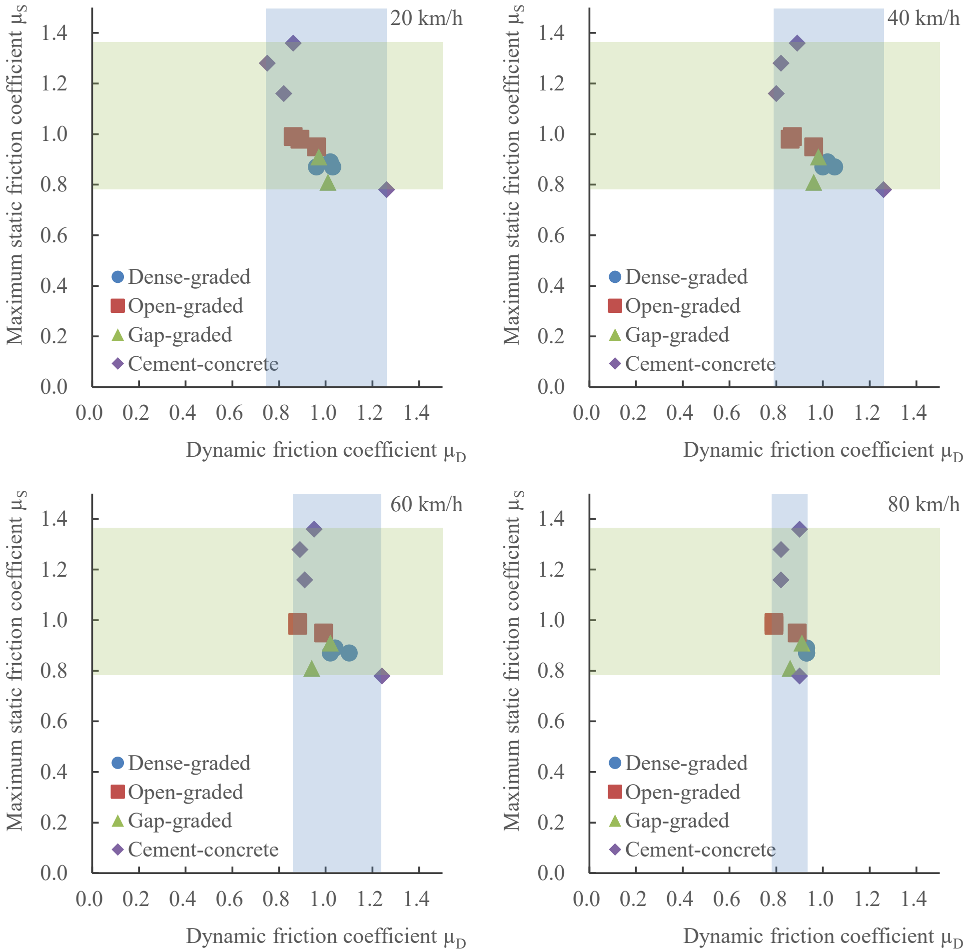

Figure 16. Relationship between dynamic friction coefficient and maximum static friction coefficient

At a sliding speed of 20 km/h, the coefficient of determination between the dynamic friction coefficient and the maximum static friction coefficient was $R^2 = 0.6187$, indicating a moderate correlation. However, the value decreased to $R^2 = 0.5002$ at 40 km/h, $R^2 = 0.3337$ at 60 km/h, and $R^2 = 0.1317$ at 80 km/h, demonstrating that the correlation weakens as the sliding speed increases. This trend likely occurs because lower sliding speeds approximate the testing conditions of portable skid resistance testers more closely.

Furthermore, examining the ranges of values for both coefficients reveals that the dynamic friction coefficient spans a narrower range than the maximum static friction coefficient, particularly at a sliding speed of 80 km/h. In other words, even among pavement surfaces with identical dynamic friction coefficients, their maximum static friction coefficients tend to vary, a tendency that becomes more pronounced at higher sliding speeds.

Conclusions

This study evaluated road surface characteristics by focusing on the maximum static friction coefficient – the value observed when a tire transitions from a rotating to a sliding state. The maximum static friction coefficient was compared with the dynamic friction coefficient based on the friction mechanisms at the tire–road interface.

The results revealed that the dynamic friction coefficient (measured via DFT) and the maximum static friction coefficient (measured using a portable skid resistance tester) exhibited contrasting trends depending on the pavement surface texture. The dynamic friction coefficient was higher on smooth surfaces, whereas the maximum static friction coefficient was higher on rough surfaces. This indicates that smooth surfaces provide shorter braking distances for a sliding tire, whereas rough surfaces offer higher resistance to the onset of tire sliding.

Furthermore, little correlation was observed between the dynamic and maximum static friction coefficients. Because the maximum static friction coefficient spans a wider range of values than the dynamic friction coefficient, surfaces with identical dynamic friction coefficients can exhibit different maximum static friction coefficients. This implies that even among surfaces that yield similar braking distances, the susceptibility of a tire to initiate sliding differs.

While conventional pavement management has relied on the dynamic friction coefficient – which focuses primarily on braking distance – evaluating the maximum static friction coefficient enables the assessment of a surface's resistance to initial tire skidding.

Although this study focused on dry road surfaces, skidding can occur even under dry conditions due to factors such as high-speed driving or driver error. Given that wet accidents remain a critical concern, future research will investigate tire–road friction mechanisms under wet surface conditions.

Disclosure statement

The authors have no conflicts of interest to declare.

Statement of the use of generative AI and AI-assisted technologies in the writing process

An AI technology was partially used to translate the original manuscript into English for this paper. In the process, AI tools were used to make revisions to the linguistic expression. AI technology was not used to create or collect any of the diagrams, pictures, and other figures used in the paper. AI technology was not used for the measured data, research findings, or analysis process. Furthermore, AI tools played no role in text generation or any part of the research process. AI technology was not used to gather references or conduct research for this paper.

REFERENCES

Abe, Y. (2000). *Study on the development and application of portable skid resistance measuring devices for road surfaces* [Doctoral dissertation, Muroran Institute of Technology].

American International. (2020). *ASTM E274, Standard test method for skid resistance of paved surfaces using a full-scale tire*.

American International. (2019). *ASTM E1911, Standard test method for measuring paved surface frictional properties using the dynamic friction tester*.

Brungraber, R. (1976). *An overview of floor slip-resistance research with annotated bibliography*. National Bureau of Standards, Technical Note 895.

Giles, C. G. (1964). *Development and performance of the portable skid-resistance tester* (Road research technical paper No.66).

Hall, J. W., Smith, K. L, & Titus-Glover, L. (2009). *Guide for pavement friction*. Washington, DC, The National Academies Press. https://doi.org/10.17226/23038

Henry, J. J. (2000). *Evaluation of pavement friction characteristics*. NCHRP Synthesis 291, Transportation Research Board.
https://onlinepubs.trb.org/onlinepubs/nchrp/nchrp_syn_291.pdf

Hirasawa, M. (2003). *Friction measurement methods and the correlation between road friction and traffic safety* (Monthly report of the Civil Engineering Research Institute of Hokkaido, No.596), 53–71.

Ichihara, K. (1969). *Studies of skidding resistance on road surfaces (1) - Ordinary road surfaces.* Public Works Research Institute Report, Vol. 135, 37–109.

Japan Road Association. (2019). *The manual for pavement survey and testing methods [1], S021-3: Method for measuring coefficient of kinetic friction on surface using skid resistance tester based on rotating*.

Li, S., Zhu, K., Noureldin, S., & Harris, D. (2005). Identifying friction variations with the standard smooth tire for network pavement inventory friction testing. *Transportation Research Record: Journal of the Transportation Research Board*, *1905*(1), 157–165.
https://doi.org/10.1177/0361198105190500117

Ono, H. (2004). Development of portable slip meter (ONO-PPSM). *Journal of Structural and Construction Engineering (Transactions of AIJ)*, *69*(585), 51–56.
https://doi.org/10.3130/aijs.69.51_4

Onoda, M. (2003). Skid resistance on road surfaces. *ASPHALT*, *46*(214), 3–10.

Saito, K. (2003). Standardization of measurement methods and measurements of skid resistance of road surface. *ASPHALT*, *46*(214), 11–18.

Sakai, H. (1979). Mechanical characteristics of tires. *Nippon Gomu Kyokai*, *52*(1), 19–33.

Smadi, O., & Alhasan, A. (2025). *Impact of pavement friction on traffic safety, Phase I: Pavement friction evaluation* (Project 19-719, Final Report), Iowa State University Institute for Transportation.

Viner, H., Sinhal, R., & Parry, T. (2004). *Review of UK skid resistance policy*. Paper prepared for 5th International Symposium on Pavement Surface Characteristics – Road and Airports.

Wallman, C., & Åström, H. (2001). *Friction measurement methods and the correlation between road friction and traffic safety: A literature review.* Report of the Swedish National Road and Traffic Institute.

Wambold, J. C., Antle, J. E., Henry, J. J., & Rando, Z. (1995). *International PIARC experiment to compare and harmonize texture and skid resistance measurements* (PIARC Report 01.04), Paris, France.